Intergranular corrosion susceptibility of Al-Cu-Li alloys

Mariana X. MILAGRE[1], Caruline S.C. MACHADO[2], João Victor ARAUJO[3], Antonello ASTARITA[4], Nadine PÉBÈRE[5], Vincent VIVIER[6], Isolda COSTA[7]

[1]*Instituto de Pesquisas Energéticas e Nucleares, Centro de Ciência e Tecnologia de Materiais, São Paulo, Brazil, marianamiagre@yahoo.com.br*
[2]*Instituto de Pesquisas Energéticas e Nucleares, Centro de Ciência e Tecnologia de Materiais, São Paulo, Brazil, carulinemachado@yahoo.com.br*
[3]*Instituto de Pesquisas Energéticas e Nucleares, Centro de Ciência e Tecnologia de Materiais, São Paulo, Brazil, joao-neutron@hotmail.com*
[4]*Dipartimento di Ingegneria Chimica dei Materiali e della Produzione Industriale, Università degli Studi di Napoli Federico II, Napoli, Italy,* antonello.astarita@unina.it
[5]*Université de Toulouse, CIRIMAT, UPS/INPT/CNRS, Toulouse, France,* nadine.pebere@ensiacet.fr
[6]*Laboratoire Interfaces et Systèmes Électrochimiques, UPR 15 du CNRS, Université Pierre et Marie Curie, Paris, Franc,* vincent.vivier@upmc.fr
[7]*Instituto de Pesquisas Energéticas e Nucleares, Centro de Ciência e Tecnologia de Materiais, São Paulo, Brazil, icosta@ipen.br*

Abstract

In the present study, the intergranular corrosion (IGC) susceptibility of commercial Al-Cu-Li alloys of the third generation (AA2098-T351, AA2198-T3 and AA2198-T851) was compared with that of the AA2024-T3 alloy according to ASTM G110 test. In addition, anodic and cathodic polarization curves were carried out in the ASTM G110 test solution at room temperature. The cross-section of the samples after the ASTM G110 test was observed by scanning electron microscopy (SEM) to evaluate the extension of the corrosion attack. The susceptibility to intergranular attack of the tested alloys was ranked according to the attack by IGC and from the anodic and cathodic polarization curves. The results showed that the AA2024-T3 and the AA2198-T3 alloys presented higher susceptibility to intergranular corrosion comparatively to the other alloys tested (AA2098-T351 and AA2198-T851). The AA2098-T351 alloy was associated to the highest resistance to intergranular attack among the alloys evaluated. A correlation was seemingly established between the stress relief treatment of the alloy and its corresponding susceptibility to intergranular or intragranular corrosion.

Key-words: intergranular corrosion; aluminum–lithium alloys; polarization curves.

1.Introduction

Aluminum alloys are largely applied in the automotive and aerospace industries. The Al-Cu-Li are high strength-density ratio alloys in reason of the precipitation-hardening treatment. The addition of lithium to aluminum provides reduction in density and an increase in elastic modulus which is attributed to the formation of intermetallic phases.

The main strengthening phase in Al-Cu-Li alloys has been reported as T_1 phase (Al_2CuLi) [1-6]. Other phases, like θ' (Al_2Cu), T_2 (Al_5Li_3Cu), T_B (Al_7Cu_4Li), S (Al_2CuMg), δ'(Al_3Li) and dispersoid particles, such as Al_3Zr and $Al_{20}Cu_2Mn_3$, may also

be present in the microstructure. The formation of these phases is mainly related to the lithium to copper ratio. Other solute elements contents and the thermomechanical history of the alloy also influence their corrosion behavior [1-6].

The Al-Cu-Li alloys present high reactivity in corrosive environments and this has been related to the presence of anodic and cathodic phases which precipitate at the grain boundaries and grow during heat treatment [1, 2, 5, 6, 14-16]

The aluminium alloys usually present good corrosion resistance in mild environments due to the oxide passive film naturally formed during air exposure. However, in chloride-containing media, aluminum alloys are susceptible to various forms of localized corrosion, for instance, intergranular corrosion (IGC) and stress corrosion cracking (SCC). This is explained by a localized attack of the oxide film stimulated by Cl^- ions [10-16].

Intergranular corrosion (IGC) is a preferential corrosive attack at the grain boundaries (GB) or at GB adjacent regions, without appreciable attack of the grain matrix. According to Galvele and de Michelli [17], IGC of Al-Cu alloys occurs only under the following conditions: (1) the alloy must have a solute-depleted zone along the grain boundaries; (2) the corrosive medium should contain anions capable of breaking down the passivity of the grain bodies; (3) the breakdown potential of the depleted zone must be lower than that of the Al; (4) the corrosion potential of the alloy must be over the breakdown potential of the depleted zone, and under the breakdown potential of the grain bodies.

The IGC susceptibility of conventional aluminum alloys, such as the AA2024-T3, has been previously reported [10,13,18]. It is related to the anodic behavior of the grain boundaries or their vicinity relative to the matrix. In the 2024 alloy, the S phase preferentially precipitates at the GB comparatively to the matrix. Besides, the precipitate free zone (PFZ) surrounding the GB promotes grain boundaries attack leading to high IGC susceptibility. The precipitates anodic to the PFZ and the matrix are preferentially attacked.

Zhang and Frankel [19] showed the influence of heat treatment on the IGC susceptibility of the AA2024 alloy. According to these authors, the breakdown potentials associated to IGC are independent on sample orientation but artificial aging had a strong effect on the alloy polarization and localized corrosion morphology. Knight *et al.* [20] showed that the thermomechanical processing leads to accelerated growth of particles at grain boundaries and a PFZ adjacent to them. Depending on the alloy and its thermal history, these PFZ can be more active than the grain and this strongly affects the IGC resistance. According to Little *et al.* [14], Cu in solid solution in Al alloys is directly correlated to the pitting potential of the Al–Cu alloy. Consequently, Cu depletion at grain boundaries due to diffusion controlled precipitation, besides growth of Cu-containing precipitates at GB, reduced pitting/repassivation potentials in the GB region compared to the bulk leading to IGC. Posada *et al.* [21] also indicated the reduction in copper content as a cause for IGC. Ma *et al.* [22] found that IGC developed from pits associated with intermetallic particles.

Relative to Al-Cu-Li alloys, Ambat e Dwarakadasa [1] found a dependence of IGC susceptibility with pH. High corrosion rates were observed in strongly acidic/alkaline

chloride solutions. Besides, in neutral pH solutions, the authors detected extensive pitting and localized attack. Kumai *et al.*, [23] also reported the influence of copper depleted zones as a cause of IGC in Al-Cu-Li alloys. Other authors proposed that IGC is caused by galvanic-couple between T_1, θ' and the PFZ [24-26].

Liu *et al.* [14] showed that the intergranular corrosion resistance properties of Al–Cu alloys decreased with increasing aging time. Proton, *et al.* [6] observed that aging treatments in Al-Cu-Li alloys resulted in formation and growth of intergranular T_1 precipitates, decreasing the copper content in solid solution. As a result of aging, the electrochemical behavior of grains differed from that of the GB explaining the IGC evolution. However, according to Guérin *et al.* [27] the T_1 phase does not necessarily induces IGC susceptibility in the AA2050-T34 alloy.

Electrochemical techniques are very useful in analyzing corrosion phenomena. Keddam *et al.* [13] evaluated the resistance of aluminum alloys to exfoliation corrosion based on the ASTM G34 standard and electrochemical impedance spectroscopy. Polarization techniques have also been used with success by many researchers to explain corrosion phenomena, including resistance to IGC [16, 19, 30-34].

The evaluation of the susceptibility of Al-Cu-Li alloys of the third generation is of great interest to the aeronautic sector however has not yet been evaluated. This is the aim of the present work where the corrosion resistance to IGC of two Al-Cu-Li alloys (2098 and 2198) with different heat treatment conditions (T3, T351, and T851) was investigated and compared with that of the AA2024-T3 aluminum alloy.

2.Experimental

The chemical compositions of the Al-Cu-Li alloys used in this work are given in Table 1. A brief description of the heat treatments of the different alloys tested is reported in Table 2.

Table 1 - Chemical composition by ICP-AES (Inductively Coupled Plasma - Atomic Emission Spectroscopy) of different Al-Li-Cu alloys in wt%

	Al	Cu	Li	Mg	Ag	Zr	Fe	Si	Zn	Mn	Cu/Li
AA2024-T3	93.5	4.2	-	1.6	-	-	0.20	0.10	0.20	0.40	-
AA2098-T351	94.5	3.4	1.0	0.3	0.3	0.4	0.04	0.05	0.02	0.003	3.4
AA2198-T3	94.6	3.3	1.0	0.3	0.3	0.4	0.04	0.06	0.02	0.003	3.3
AA2198-T851	94.6	3.4	1.0	0.3	0.3	0.4	0.04	0.04	0.01	-	3.4

Table 2 – Heat treatments for the aluminum alloys used in this study.

Heat treatment condition	Description
T3	(1) Solution heat treated; (2) cold worked; (3) naturally aged.
T351	(1) Solution heat treated; (2) stress relieved by stretching (3) naturally aged.
T851	(1) Solution heat treated; (2) stress relieved by stretching; (3) artificially aged.

The intergranular corrosion susceptibility test was performed by following the ASTM G110-92 [29]. Prior to immersion, the specimens surface was prepared according to: (1) immersion for 1 minute in etching solution, composed by 945 mL of deionized water, 50 mL of nitric acid (70 %) and 5 mL of hydrofluoric acid; (2) rinsing in deionized water; (3) immersion for 1 minute in concentrated nitric acid (70 %); (4) rinsing in deionized water and (5) drying under hot air stream. After surface preparation, the specimens were immersed for 12 hours in the test solution composed by 1L of

deionized water, 57 g of NaCl and 10 mL of H_2O_2. The volume/area ratio of the test solution used was 5 mL/cm^2. The area exposed to the test solution corresponded to 20 mm x 20 mm.

The ASTM G110-92 standard practice consists on immersing aluminum alloys in a sodium chloride with hydrogen peroxide solution for six or more hours. After this period, the metallographic sections of the exposed samples were observed to determine the extent of intergranular corrosion. This practice may be used to study the effect of thermal processes or precipitation treatments on the corrosion resistance [29]. However, this practice is based on examination of the alloy surface by microscopy the observation being of a qualitative type. Quantitative measurements may assist the evaluation of intergranular corrosion susceptibility of aluminum alloys. In the present study, electrochemical techniques (polarization curves) were used to help investigate the susceptibility of the alloys to IGC.

Polarization curves were obtained by using an AUTOLAB PGSTAT potentiostat controlled by NOVA 1.11 software. The tests were performed at room temperature using a three electrode-cell experimental setup. The working electrode corresponded to the alloy with an exposed surface area of 1 cm^2, the $Ag/AgCl_{KCl(sat)}$ electrode was used as reference and a platinum wire acted as counter electrode. Anodic and cathodic polarization curves were obtained separately, from the open circuit potential (OCP) up to 0.5 V vs. $Ag/AgCl_{KCl(sat)}$ with a scan rate of 1 mV/s**.** After the tests, the cross section of the samples and the surface exposed to the test solution were analyzed by scanning electron microscopy (SEM) using a Hitachi TM 3000 microscope with an incident beam of 15 keV.

3. Results and Discussion

Figure 1 shows the variation of OCP as a function of exposure time to the corrosion test solution (1L of deionized water, 57 g of NaCl and 10 mL of H_2O_2).

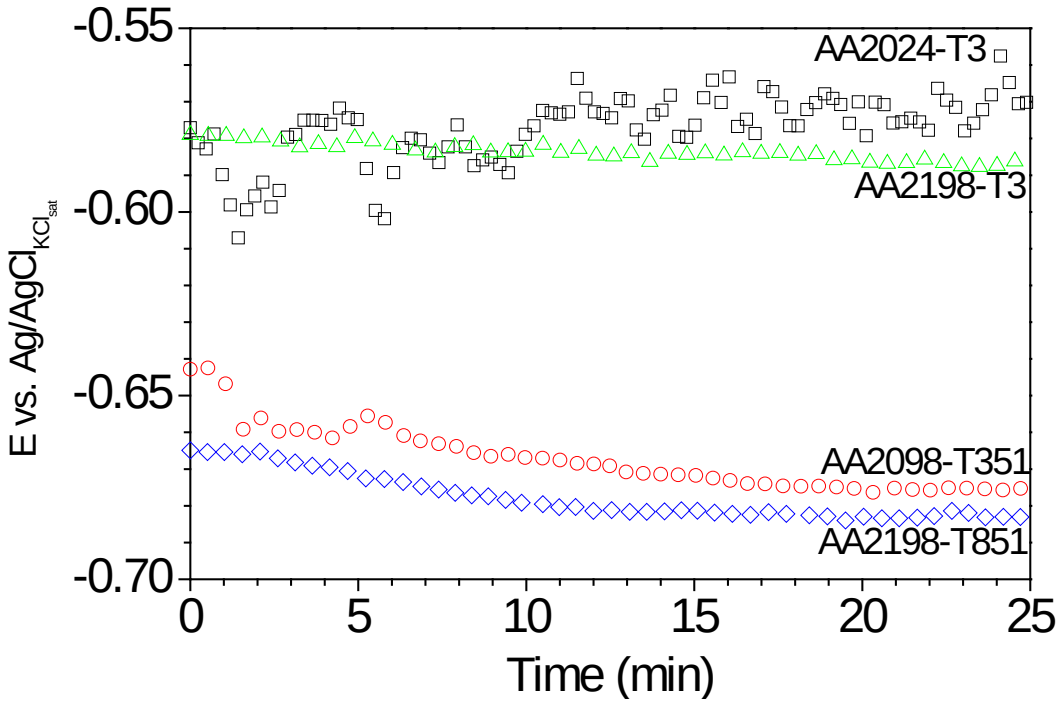

Fig. 1. Open circuit potential as a function of time of exposure in 1L of deionized water, 57 g of NaCl and 10 mL of H_2O_2.

The oscillations in OCP during the exposure to the test solution for the 2024-T3 alloys indicate a high instability of this alloy in the ASTM G110 solution showing its high corrosiveness. The increase in the OCP for the 2024 alloy with time is explained by Cu enrichment at the surface along the corrosion attack. Copper is much nobler than aluminum and lithium and consequently, during corrosion dissolution, accumulates at the exposed surface leading to OCP ennoblement. Despite of the similar compositions of the Al-Cu-Li alloys tested, the OCP values corresponding to the 2198-T3 alloy was higher than that of the two other Li containing alloys and it was close to the one of the 2024-T3 one. The OCP for the 2198-T3 alloy decreased with time, as it was observed for the other Al-Cu-Li alloys. This result shows a solid effect of the heat treatment on OCP data. The OCP decrease with time for all the Al-Cu-Li alloys is likely associated to the increasingly depolarization of the anodic reactions in these alloys resulting in progressively attack of the surface, as in fact it was observed. Potentials in the range from -0.56 to -0.58 V were measured after 30 min of exposure to the solution for the 2024-T3 and 2198-T3 alloys, and the literature reports pitting and intergranular corrosion for aluminium alloys at this range of potential [7,12].

Anodic and cathodic polarization curves obtained separately are shown in Figure 2 (a) and (b), respectively. Instabilities were observed for the 2024-T3 alloy in the anodic polarization curves and a breakdown potential was not clearly indicated for this alloy, indicating that the OCP was above its pitting potential. All Al-Cu-Li alloys showed a breakdown potential but oscillations typical of surface instability was also observed for the 2198-T3 alloy. The lowest corrosion currents were associated to the 2098-T351 alloy indicating a better stability of this alloy comparatively to the others in the test solution.

For the 2024-T3 alloy, diffusion controlled cathodic reactions are clearly indicated in the cathodic polarization curves whereas for the Al-Cu-Li alloys a mixed control was suggested for low overpotential but diffusion controlled cathodic reaction was indicated for the 2198-T3 alloy at higher overpotentials. The highest cathodic currents were related to the 2024-T3 alloy whereas the lowest to the 2098-T351. For this last alloy, the shape of the cathodic curve was very similar to that of the 2198-T851 suggesting similar cathodic mechanisms for the 2098-T351 and 2198-T851 alloys.

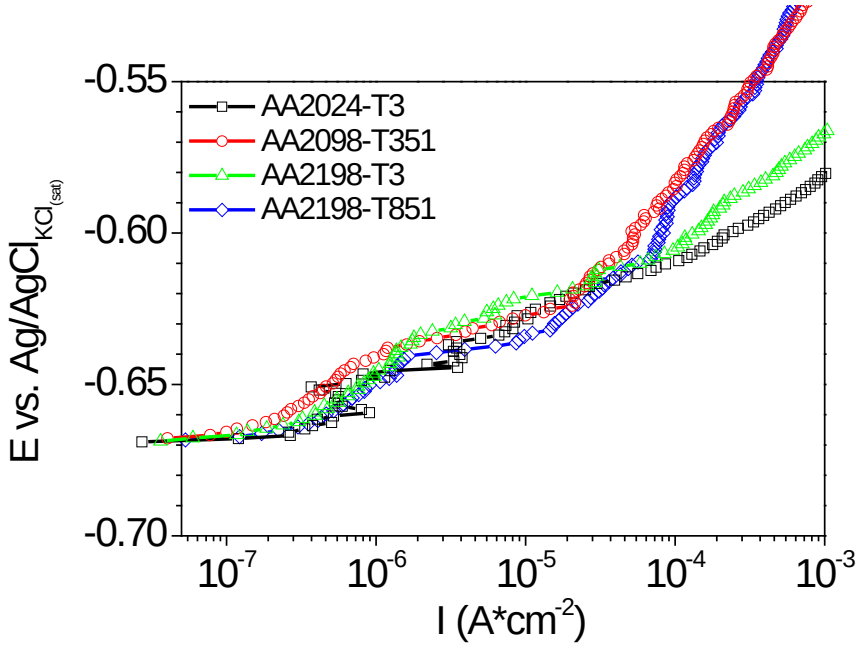

(a)

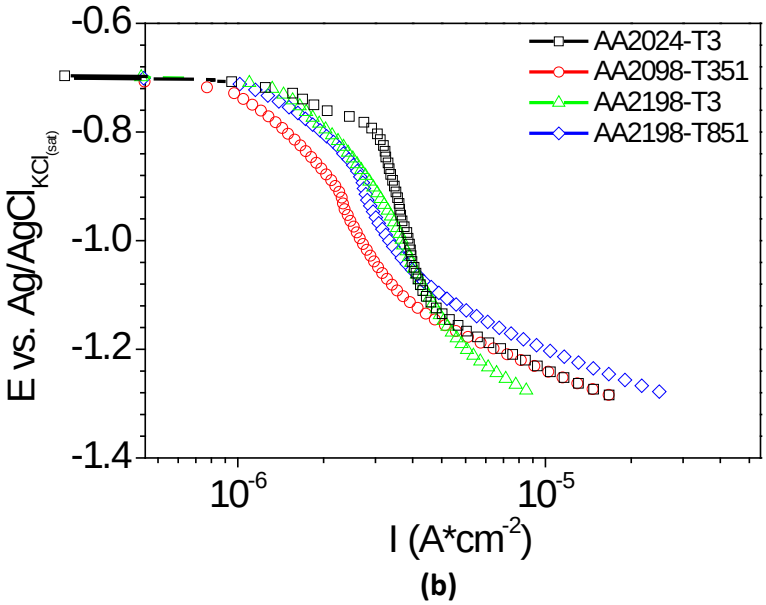

(b)

Fig. 2. Polarization curves obtained after 30 min exposure to test solution (1L of deionized water, 57 g of NaCl and 10 mL of H_2O_2), normalized in relation to the lowest OCP measured for all alloys. (a) Anodic polarization curves and (b) cathodic polarization curves.

Figure 3 shows the cross section view of the various tested alloys exposed for 12 h to the intergranular corrosion solution.

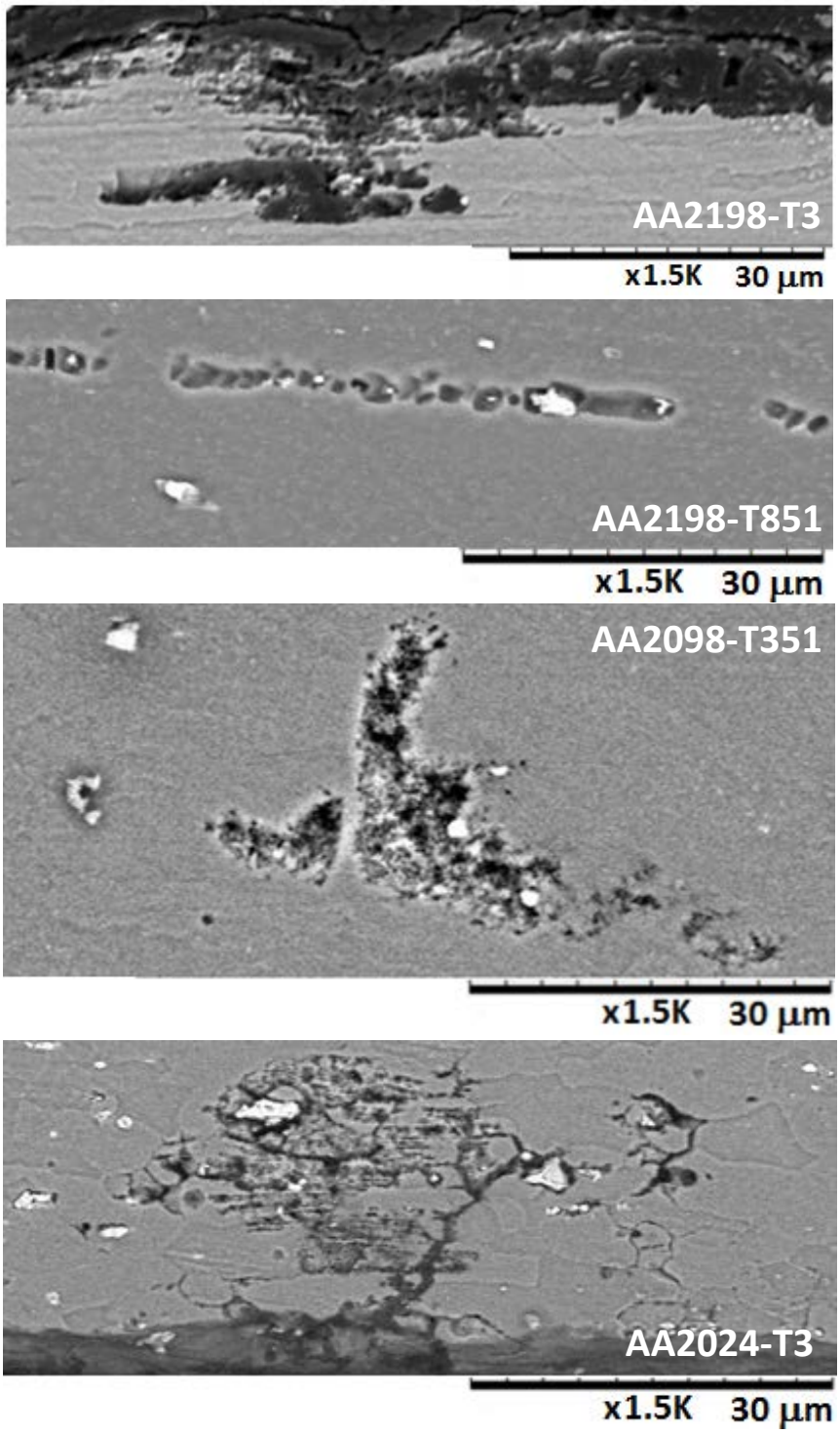

Fig. 3. Cross-section view of various samples exposed for 12 h to the intergranular corrosion test solution (1 L of deionized water, 57 g of NaCl and 10 mL of H_2O_2).

The Al-Cu-Li alloys showed different intergranular corrosion resistances despite their similar chemical compositions (Table 1). Penetration of corrosion into the alloy through the grain boundaries was observed for the 2024-T3 and 2198-T3 alloys. Luo *et al.* [28] observed that intergranular corrosion initiated from the corrosion pit bottom, connects

to the corrosion pit via small openings, and developed into the large network buried underneath the alloy surface. For Al-Cu-Li alloys, remnant T_1 phase precipitates and corroded IM particles at grain boundaries induced dissolution in the periphery of the particle, and promoted intergranular corrosion propagation. During GB attack, copper accumulates at the corrosion products at the aluminum matrix interface in the intergranular corrosion filament. Subsequently, the copper enriched band acts as local cathodes supporting reduction reactions. This would explain the differentiated electrochemical behavior of the 2198-T3 alloys comparatively to the other Al-Cu-Li alloys tested. On the other hand, the corrosion attack on the 2198-T851 and 2098-T351, that is, the samples exposed to stress relief treatments, seemingly occurred inside the grains, showing a intragranular attack. Cu rich particles precipitation is favored by the T3 heat treatment. Particles precipitation occurs preferentially in the T3 (natural aging) condition than in the T8 condition since a rapid quench rate after solution heat treatment maintains most of the alloying elements in solid solution, while a slow rate favors precipitation of some alloying elements as hardening particles [22].

It is well known that microstructural changes occur during solution heat treatment. Artificial aging changes the mechanical properties and corrosion behavior of the alloy. The changes include particle dissolution, particle coarsening, precipitation, changes in dislocation distribution and density, as well as changes of composition and structure in subgrain and grain boundaries [10]. Fig. 3 suggests that artificial aging changed the corrosion morphology of the alloy from intergranular to intragranular and decreased the corrosion potential of the alloy [6]. This is attributed to presence of T_1 precipitates inside the grains and a decrease in Cu content in the matrix phase.

The stress relief by stretching is seen to modify the corrosion morphology and electrochemical response of the alloys naturally aged. The corrosion behavior of Al–Cu–Li alloys is related to the distribution of T_1 precipitates. These particles nucleate preferentially on dislocations and at subgrain/grain boundaries [6]. Solute segregation in grain boundaries due to low cooling rates favors T_1 precipitation, and the stretching changes the dislocation distribution, dislocation density and the composition of grain and subgrain boundaries. In the case of artificially aged alloys, like T851 treatments, T_1 precipitation is favored in grain bulk and no significant intergranular corrosion is observed. Due to fast cooling rates in artificially aged alloys, more elements are in solid solution, and precipitation occurs mainly in the matrix. Thus, a stress relief treatment increased the resistance of the Al-Cu-Li alloys to intergranular corrosion and favors the intragranular attack.

4. Conclusions

The AA2024-T3 and AA2198-T3 alloys presented higher susceptibility to intergranular corrosion comparatively to the AA2098-T351 and AA2198-T851 alloys. The first alloys showed similar electrochemical and IGC resistance whereas alloys with similar chemical composition but different treatments (T-351 and T-851) were susceptible to intragranular attack. The introduction of a stress relief treatment by stretching resulted in increased resistance to IGC.

Acknowledgments

The authors acknowledge CAPES (Capes/Cofecub N°806-14) and FAPESP (2013/13235-6) for financial support for this work and to CAPES for the grants of M.X.Milagre (99999.000332/2016-00) and C.S.C. Machado (99999.000400/2016-05).

References

1. R. Ambat, E. S. Dwarakadasa, Corrosion Science, **33** (1992) 681.
2. J. P. Moran, E. A. Starke Jr., G. E. Stoner, G. L. Cahen, Jr., Corrosion, **43** (1987) 374.
3. Jing Gui, T. M. Devine, Scripta Metallurgica, **21** (1987) 853.
4. J. Martin, Materials Science, **18** (1988) 101.
5. P. Niskanen, T. H. Sanders Jr., J. G. Rinker, M. Marek, Corrosion Science, **22** (1982) 283.
6. V. Proton, J. Alexis, E. Andrieu, J. Delfosse, A. Deschamps, F. de Geuser, M. Lafont, C. Blanc, Corrosion Science **80** (2014) 494.
7. P. S. De, Mishra, J.A. Baumann, Acta Materialia, **59** (2011) 5946.
8. R. J. Rioja, J. Liu, Metallurgical and Materials Transactions A, **43A** (2012).
9. P.S. Chen and B. N. Bhat. NASA/TM--2002-211548, 2012.
10. V. Guillaumin, G. Mankowski, Corrosion Science, **41** (1999) 421.
11. H. Li, D. Huang, W. Kang, J. Liu, Y. Ou, D. Li, Journal of Materials Science & Technology, **32** (2016), 1049.
12. C. Blanc, A. Freulon, M. Lafont, Y. Kihn, G. Mankowski, Corrosion Science, **48** (2006) 3838.
13. M. Keddam, C. Kuntz, H. Takenouti, D. Schuster, D. Zuili, Electrochimica Acta, **42**, (1997) 87.
14. D. A. Little, B. J. Connolly, J. R. Scully, Corrosion Science, **49** (2007) 347.
15. W. Zhang, G. S Frankel, Electrochemical and Solid-State Letters, **3** (2000) 268.
16. O. Jilani, N. Njah, P. Ponthiaux, Corrosion Science **87** (2014) 259.
17. J. R. Galvele, S. M. de Michelli, Corrosion Science, **10** (1970) 795.
18. M. J. Robinson, Corrosion Science, **22** (1982) 775.
19. W. Zhang, G. S. Frankel, Electrochimica Acta, **48** (2003) 1193.
20. S.P. Knight, M. Salagaras, A. R. Trueman, Corrosion Science **53** (2011) 727.
21. M. Posada, L. E. Murr, C. S. Niou, D. Roberson, D. Little, R. Armwood, D. George, Materials Characterization, **38** (1997) 259.
22. Y. Ma, X. Zhou, G. E. Thompson, M. Curioni, X. Zhong, E. Koroleva, P. Skeldon, P. Thomson, M. Fowles, Corrosion Science**, 53** (2011) 4141.
23. C. Kumai, Corrosion Science, **45** (1989) 294.
24. Y. Xu, X. Wang, Z. Yan, J. Li, Chinese Journal of Aeronautics, **24** (2011) 681.
25. W. Liang, Q. Pan, Y. He, Y. Li, Y. Zhou, C. Lu, Rare Metals, **27** (2008) 146
26. Y. Li, W. Kang X. C. Lu, Journal of Alloys and Compounds, **640** (2015) 210.
27. M. Guérin, J. Alexis, E. Andrieu, L. Laffont, W. Lefebvre, G. Odemer, C. Blanc, Corrosion Science, **102** (2016) 291.
28. C. Luo, Corrosion Science, **61** (2012) 35.
29. ASTM International. ASTM G110-92: Standard Practice for Evaluating Intergranular Corrosion Resistance of Heat Treatable Aluminum Alloys by Immersion in Sodium Chloride + Hydrogen Peroxide Solution, 1992;

30. Y. Ma, X. Zhou, X. Meng, W. Huang, Y. Liao, X. Chen, Y. Yi, X. Zhang, G. E. Thompson, Trans. Nonferrous Met. Soc. China, **26** (2016) 1472.
31. N. D. Alexopoulos, Z. Velonaki, C. I. Stergiou, S. K. Kourkoulis, Corrosion Science **102** (2016) 413.
32. X. Y. Liu, M. J. Li, F. Gao, S. X. Liang, X. L. Zhang, H. X. Cui, Journal of Alloys and Compounds, **639** (2015) 263–267.
33. A. S. El-Amoush, Materials Chemistry and Physics **126** (2011) 607.
34. C. Li, Q. Pan, Y. Shi, Y. Wang, B. Li, Materials and Design, **55** (2014) 551–559
35. K. S. Ghosh, K. Das, U. K. Chatterjee, Metallurgical and Materials Transactions A, **35A** (2004) 3683.
36. T. D. Burleigh, R. C. Rennick, F.S. Bovard, Corrosion, **49** (1993) 683.